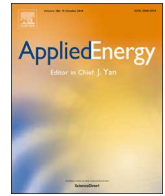




ELSEVIER

Contents lists available at ScienceDirect

Applied Energy

journal homepage: www.elsevier.com/locate/apenergy

A hot syngas purification system integrated with downdraft gasification of municipal solid waste



Wei Ping Chan^{a,*}, Andrei Veksha^a, Junxi Lei^a, Wen-Da Oh^{a,b}, Xiaomin Dou^a, Apostolos Giannis^{a,c}, Grzegorz Lisak^{a,d}, Teik-Thye Lim^{a,d,*}

^a Residues and Resource Reclamation Centre, Nanyang Environment and Water Research Institute, Nanyang Technological University, 1 Cleantech Loop, Clean Tech One, 637141, Singapore

^b School of Chemical Sciences, Universiti Sains Malaysia, 11800 Penang, Malaysia

^c School of Environmental Engineering, Technical University of Crete (TUC), Politechniopolis, 73100 Chania, Greece

^d School of Civil and Environmental Engineering, Nanyang Technological University, 50 Nanyang Avenue, Singapore 639798, Singapore

HIGHLIGHTS

- Demonstrated feasibility of MSW gasification with a hot syngas purification system.
- Produced hot and clean syngas through downward cascading of system temperatures.
- Removed up to 90% of tar compounds and sulfur species (H₂S and COS).
- Demonstrated operational stability of Ni/Al₂O₃ catalyst for over 20 h on stream.
- Demonstrated reliable performance of NiZn-28-HC sorbent with real MSW syngas.

ARTICLE INFO

Keywords:

Syngas purification
Municipal solid waste
Catalytic tar reforming
Nickel catalyst
Ni-Zn nanocomposite
Sulfur removal

ABSTRACT

Gasification of municipal solid waste (MSW) with subsequent utilization of syngas in gas engines/turbines and solid oxide fuel cells can substantially increase the power generation of waste-to-energy facilities and optimize the utilization of wastes as a sustainable energy resources. However, purification of syngas to remove multiple impurities such as particulates, tar, HCl, alkali chlorides and sulfur species is required. This study investigates the feasibility of high temperature purification of syngas from MSW gasification with the focus on catalytic tar reforming and desulfurization. Syngas produced from a downdraft fixed-bed gasifier is purified by a multi-stage system. The system comprises of a fluidized-bed catalytic tar reformer, a filter for particulates and a fixed-bed reactor for dechlorination and then desulfurization with overall downward cascading of the operating temperatures throughout the system. Novel nano-structured nickel catalyst supported on alumina and regenerable Ni-Zn desulfurization sorbent loaded on honeycomb are synthesized. Complementary sampling and analysis methods are applied to quantify the impurities and determine their distribution at different stages. Experimental and thermodynamic modeling results are compared to determine the kinetic constraints in the integrated system. The hot purification system demonstrates up to 90% of tar and sulfur removal efficiency, increased total syngas yield (14%) and improved cold gas efficiency (12%). The treated syngas is potentially applicable in gas engines/turbines and solid oxide fuel cells based on the dew points and concentration limits of the remaining tar compounds. Reforming of raw syngas by nickel catalyst for over 20 h on stream shows strong resistance to deactivation. Desulfurization of syngas from MSW gasification containing significantly higher proportion of carbonyl sulfide than hydrogen sulfide, traces of tar and hydrogen chloride demonstrates high performance of Ni-Zn sorbents.

* Corresponding authors at: Residues and Resource Reclamation Centre, Nanyang Environment and Water Research Institute, Nanyang Technological University, 1 Cleantech Loop, Clean Tech One, 637141, Singapore (T.-T. Lim).

E-mail addresses: wpchan@ntu.edu.sg (W.P. Chan), cttlim@ntu.edu.sg (T.-T. Lim).

<https://doi.org/10.1016/j.apenergy.2019.01.031>

Received 14 September 2018; Received in revised form 19 November 2018; Accepted 2 January 2019

Available online 08 January 2019

0306-2619/© 2019 The Authors. Published by Elsevier Ltd. This is an open access article under the CC BY license (<http://creativecommons.org/licenses/by/4.0/>).

Nomenclature

GS	downdraft fixed-bed gasifier
TR	fluidized-bed catalytic tar reformer
DES	fixed-bed reactor for sulfur removal
MSW	municipal solid waste
RDF	refuse-derived fuel
CGE	cold gas efficiency
WtE	Waste-to-Energy
CCGT	combined cycle gas turbine

SOFC	solid oxide fuel cell
PAH	polyaromatic hydrocarbon
ER	equivalence air ratio
A/F	air-to-fuel ratio
WGS	water-gas shift
wt%	weight percentage
vol%	volume percentage
SD	standard deviation
RSD%	relative standard deviation

1. Introduction

Global municipal solid waste (MSW) generation rate is estimated at 1.3 billion tonnes per year in 2012, and it is expected to increase to 2.2 billion tonnes annually by 2025 [1]. Incineration is commonly applied in the management of MSW to achieve 70–80% mass reduction and 80–90% volume reduction [2] while it produces electricity with up to 30% of net electrical efficiency [3]. Recently, development of different Waste-to-Energy (WtE) treatment technologies such as pyrolysis, gasification and hydrothermal processes [4] have attracted significant research interest as alternative to incineration [5]. Gasification is an advanced thermochemical conversion process which converts MSW into gaseous fuel (syngas) that can be utilized in gas engines, combined cycle gas turbines (CCGTs) [6], solid oxide fuel cells (SOFCs) [7], or hybrid systems [8] with higher electrical efficiency and better environmental performance [9] and therefore optimize the utilization of wastes as a sustainable energy resources. Formation of dioxins and furans is an important concern when MSW, particularly plastic wastes, are treated in thermochemical conversion processes. Nevertheless, as compared to incineration, reducing environment in a gasifier strongly inhibits the formation of these compounds [2]. In addition, Cl containing species (HCl, KCl and NaCl) can be removed from the syngas through the purification system, which further reduce the potential of dioxins and furans formation during the downstream applications of syngas [10]. Combustion of treated syngas as a homogenous gaseous fuel in gas engines/turbines instead of the direct combustion of highly heterogeneous MSW also reduce the formation of dioxins and furans. This is because the well-controlled complete combustion eliminates the residual carbon in the flue gas that acts as a precursor for the formation of dioxins and furans [11].

However, the main constraint of using syngas for downstream applications is the presence of high concentrations of impurities such as particulates, tar, HCl, alkali chlorides and sulfur species [12]. There are conventional and highly efficient cold clean-up systems such as venturi scrubbers, wash towers, wet/dry electrostatic precipitators, adsorbing beds or cyclones. These systems suffer from significant heat and energy efficiency losses and produce significant amount of solid and liquid waste streams [13]. Therefore, warm or hot clean-up systems are preferable to maintain high thermal efficiency of the WtE facilities and convert the impurities into potentially useful products [14].

Various warm/hot clean-up processes have been developed to remove different impurities in syngas. Particulates emitted from a gasifier consists of residual solid carbon and inorganic compounds such as alkali and alkaline earth metals, silica and trace constituents of other metals [15]. Various techniques are readily available for particulates removal such as cyclones, dust agglomerators, fabric filters, electrostatic separators and ceramic candles with removal efficiency of 99.5% or more at warm/hot temperature of 400 °C and above [16]. Chlorine species in syngas are predominantly represented as HCl, NH₄Cl and alkali chlorides which are either vapors or solids depending on the operating temperatures [13]. Sodium- and calcium minerals can be applied as sorbents for removing HCl while activated alumina and natural minerals such as kaolinite and bauxite can be used as sorbents

for removing alkali chlorides at around 400 °C or higher temperature [15].

Tar is a complex mixture of organic compounds with molecular weight greater than that of benzene. It consists of oxygenated products, heavier deoxygenated hydrocarbons and polycyclic aromatic hydrocarbons (PAHs) [17]. Tar compounds can be categorized based on their chemical structure, number of carbon ring and molecular weight [18]. The categorization and identification of tar components are crucial because the concentration limits [19] and dew points [20], the two most important criteria to be considered for downstream application of syngas, are significantly affected by the specific tar compounds found in the syngas. In general, a highly efficient syngas purification system should focus on the reduction of heavier tar compounds if complete removal of tar is not cost-effective [20].

Thermal cracking at extreme temperature of 1075–1300 °C, catalytic reforming with different types of catalysts and plasma treatment are typical hot/warm tar removal technologies [15]. Catalytic tar reforming is considered as one of the most promising technologies, considering its scalability and energy efficiency, but the main limitation is catalyst deactivation [21]. In addition, catalytic tar reforming with nickel-based catalysts showed superior tar reduction performances at high temperature [22], improved heating values of syngas, increased gas yield and demonstrated catalytic conversion of NH₃ into N₂ [23]. Existing studies focus extensively on fixed bed reactor with catalysts in the shape of pellet, ring, spherical, monolith and catalytic filter [21]. Nevertheless, catalytic reforming with a fluidized bed could improve the efficiency of this process by promoting the mixing of syngas with catalyst, maintaining uniform temperature in the tar reformer and reducing potential bed agglomeration and coking [24]. Nickel particles can be supported by using different materials which include alumina [25], limestone [22], dolomite [26] and char [27] to improve the catalytic activity and maintain the stability during reforming. Alumina can be considered as a suitable support material when high temperature fluidized-bed catalytic tar reformer is applied because of its high mechanical integrity, thermal stability [25], inert to gasification reactions and strong resistance to sintering and poisoning by HCl [22].

Sulfur species in syngas are predominantly present as H₂S and COS [28]. Adsorption techniques that include chemical sorbents are commonly applied to remove sulfur. Metal oxides are typically used for high temperature desulfurization, while improvement on regenerability and removal efficiency of the sorbent materials are currently under development [15]. Advancement of hierarchical [29] and regenerable zinc oxide sorbents for syngas desulfurization suggested the potential of utilizing nanostructured materials to improve the techno-economic performance of desulfurization system [30]. Incorporation of additives (Ni, Cu, etc.) as promoters into ZnO sorbents could further enhance the desulfurization performance, increase the sorption capacity and stability, and improve the regenerability of the sorbents [31]. To further improve the applicability of sorbent, ZnO could be immobilized on a honeycomb which would minimize pressure drop and avoid pore plugging in the desulfurization reactor [28]. Regeneration of the used sorbents produces SO₂ which can be subsequently recovered as sulfuric acid [32] or elemental sulfur [33].

From the thermal efficiency perspective, positioning of catalytic tar reformer at the outlet of gasifier followed by the downward cascading of syngas temperature through the purification system is highly efficient. This arrangement reduces the need for syngas cooling and reheating, thus decreasing the cost and increasing the efficiency of purification system [34]. However, tar reforming catalysts could lose their reforming activity when directly in contact with raw syngas due to carbon and particulates deposition [35], poisoning by sulfur species, deactivation by HCl [36] and sintering [37]. On the other hand, desulfurization sorbents are difficult to be regenerated with highly consistent performance and sorbent deactivation can be accelerated due to the presence of chlorine species in syngas [29]. Our recent study has reported the synthesis of Ni/Al₂O₃ catalyst with high stability to poisoning by HCl due to the strong Ni nanoparticle-support interactions and nano-sized porous alumina support [22]. Additionally, Ni-Zn oxide nanocomposites have been developed with good regenerability and high sulfur capacity compared to pure ZnO in model syngas [28]. However, these advanced materials have not been used previously for the purification of real MSW syngas and there is limited research in the arrangement of multi-stage system with downward cascading of temperature for the purification of real syngas produced from MSW gasifier. Therefore, testing of these novel catalysts and sorbents in real syngas with wide range of impurities through a well arranged multi-stage system is of great importance to understand the system stability and efficiency throughout the purification processes.

In this study, a novel syngas purification system is constructed to investigate the feasibility of high temperature purification of raw syngas from gasification of MSW, with the focus on catalytic tar reforming, desulfurization and the system arrangement with downward cascading of syngas temperatures. MSW, in the form of refuse-derived fuel (RDF) pellets, is gasified in a downdraft fixed-bed gasifier at 850 °C with equivalence air ratio (ER) of 0.3 and 25 wt% moisture content to produce syngas with consistent quality similar to the properties of syngas generated in industrial gasifiers. The generated raw syngas is then treated in a multi-stage purification system with downward cascading of the syngas temperature to remove impurities while producing hot and clean syngas at 400 °C as a final product. For the first time, a fluidized-bed tar reforming reactor with Ni catalysts supported on Al₂O₃ is utilized for the removal of tar from real MSW syngas containing particulates, chlorine and sulfur compounds. Particulate filter and Na₂CO₃ are installed to remove particulates and HCl prior to the desulfurization unit. The removal of sulfur species (H₂S and COS) is carried out by using Ni-Zn oxide sorbent. Efficiency of the removal of impurities, stability of catalysts and sorbents, and performance of the purification system are analyzed. Selectivity of tar reforming catalysts towards tar decomposition from MSW syngas is described. Dew points and specific contents of different tar compounds in the treated syngas are determined and compared to the operating requirements and concentration limits of the downstream application of syngas, which include gas engines/turbines and SOFCs. Complementary sampling and analysis methods are applied for tar, alkali chlorides and HCl quantification to provide insights into the distribution of these impurities throughout the multi-stage system. Experimental and thermodynamic modeling results are compared to determine the differences caused by the kinetic constraints of the multi-stage system.

2. Materials and methods

2.1. Preparation and characterization of RDF

MSW generated in Nanyang Technological University (Singapore) was used to prepare the RDF pellets. Approximately 200 kg of mixed wastes were collected from the central waste collection site. The wastes were sorted, weighed and dried according to ASTM D5231. Six main combustible components, plastic, paper, textile, wood, food residues and horticultural wastes were selected and retained to form the RDF

pellets while other waste components were discarded, which include glassware, metals, liquids, stones, ceramics and rubbers. The overall moisture content of the collected wastes was 25 wt%. After drying at 105 °C for at least 24 h, the components were crushed into pieces (Retsch SM2000 and plastic crusher, DJ400). Crushed wastes were mixed and homogenized to form a mixture with 35 wt% plastic, 25 wt% paper, 7.7 wt% textile, 6.9 wt% wood, 16 wt% food residues and 11.4 wt% horticultural wastes. Homogenized mixture was pelletized to form RDF pellets with diameter of 4 ± 1 mm and length of 10 ± 3 mm (pellet mill, Gemco). Characteristics of RDF pellets (Table S1) were determined based on the methods described previously [38].

2.2. Catalysts, filter and sorbent materials

One commercially available catalyst (Pingxiang Hualian Chemical Ceramic Co., China) and one fabricated nickel catalyst supported on alumina were used for fluidized-bed tar reforming. For the catalyst fabrication, aluminum hydroxide H₃AlO₃·xH₂O (Sigma-Aldrich) was pelletized and the prepared pellets were crushed to obtain particles with sizes 0.56–1.18 mm. Approximately 17.2 g of particles were added to the solution containing a known quantity of Ni(NO₃)₂·6H₂O (Sigma-Aldrich) in 10 mL deionized water and mixed. The solvent was evaporated using a rotary evaporator Hei-Vap Precision (Heidolph Instruments). The material was dried overnight in an oven at 105 °C and then calcined in air at 850 °C for 2 h (heating rate of 2 °C/min). Both commercial and fabricated catalysts were crushed and sieved to the particle size of 100 to 315 μm and are denoted as C-Cat and F-Cat, respectively. Further details on chemicals, synthesis procedure and characterization of these catalysts could be found elsewhere [22]. Bulk densities of C-Cat and F-Cat were 1.27 g/mL and 0.80 g/mL respectively. Based on the X-ray fluorescence (XRF, PANalytical Axios mAx), NiO contents for C-Cat and F-Cat were 19.9 wt% and 15.8 wt% respectively. 3 mL of the C-Cat (space velocity, SV = 6000 h⁻¹) and 3 mL, 4 mL and 5 mL of F-Cat (SV = 6000, 4500 and 3600 h⁻¹, respectively) were used in the fluidized-bed tar reformer. The effective loadings of NiO calculated from XRF data were 0.76 g for 3 mL of C-Cat and 0.38, 0.51 and 0.63 g for 3, 4 and 5 mL of F-Cat, respectively.

A quartz thimble filter (No.88R, Advantec) was used to remove particulates. CaO and Na₂CO₃ (Sigma-Aldrich) were pelletized, crushed and sieved to a particle size of 2.0–2.8 mm and used for the HCl capture.

Ni-Zn nanocomposite loaded on honeycomb (cordierite mullite), denoted as NiZn-28-HC, was applied to remove sulfur species (H₂S and COS). For the preparation of NiZn-28-HC, the honeycomb was first seeded by immersing into a seeding solution containing 20 mmol of Zn (CH₃COO)₂·2H₂O in 50 mL ethanol and 2 mL diethanolamine for 2 h [30]. The honeycomb was then slowly removed from the seeding solution, dried at 60 °C for 2 h and calcined in air at 400 °C for 2 h (heating rate of 2 °C/min). The seeded honeycomb was placed into a solution prepared from 5 mmol of Zn(NO₃)₂·6H₂O, 20 mmol of urea and 2 mmol of Ni(NO₃)₂·6H₂O in 30 mL deionized water under rapid magnetic stirring for 20 min, followed by hydrothermal synthesis at 100 °C for 18 h and calcination at 400 °C for 5 h (heating rate of 2 °C/min). Details of the synthesis and characterization of this sorbent are described in a previous study [28]. Mass of the honeycomb was 3.06 ± 0.05 g (SV = 11,500 h⁻¹) with 1.77 ± 0.02 wt% of Ni-Zn and Ni:Zn molar ratio of 2:5 on the honeycomb.

2.3. Characterization of materials

Temperature programmed reduction (TPR) was performed by flowing a 5% H₂/N₂ gas mixture at 30 mL/min and a heating rate of 10 °C/min up to 900 °C. Transmission electron and field-emission scanning electron micrographs were obtained by using JEOL microscopes (JEM-1400 and JEM 2010 for TEM and 7600F for FESEM). X-ray diffraction (XRD) patterns were obtained by using X-ray diffractometer

(Bruker AXS D8 Advance) operated with high intensity monochromatic Cu-K α source at $\lambda = 1.5418 \text{ \AA}$ at 40 kV and 40 mA. X-ray photoelectron spectroscopy (XPS) was conducted by using a spectro-photometer (Kratos Axis Supra) with a dual anode monochromatic K α excitation source. All binding energies for elements of interest were corrected against an adventitious carbon C 1s core level at 284.8 eV. XPS peaks were deconvoluted using CASA XPS software by fitting the peaks on Shirley background coupled with Gaussian-Lorentzian function.

2.4. Gasification and syngas purification system

The multi-stage purification system integrated with gasifier is illustrated in Fig. 1. A downdraft fixed-bed gasifier was used to produce raw syngas by gasifying RDF pellets with a feeding rate of approximately $4.4 \pm 0.3 \text{ g/min}$. Stoichiometric air-to-fuel (A/F) ratio was estimated as 6.96 L/g, by calculating stoichiometric balance of the complete oxidative reaction between C, H, N, S and O elements in RDF pellets and O₂ in air assuming the reaction products are CO₂, H₂O, NO₂ and SO₂. To maintain an equivalence air ratio of 0.3 and water content of 25 wt%, 9.2 L/min of air and 1.47 mL/min of deionized water were injected simultaneously into the gasifier. Approximately 12 L/min of raw syngas (on a dry basis) was generated from the gasifier and 300 mL/min of the raw syngas was directed into the purification system. The system included a fluidized-bed catalytic tar reformer, a particulate filter and a fixed-bed reactor with dechlorination and desulfurization adsorbents to remove tar, particulates, HCl and sulfur species (Fig. 2) from the raw syngas with downward cascading of the syngas temperature. Connecting lines and particulates filter were maintained at 300 °C. Pressure in the gasifier and purification system were monitored continuously throughout the experiment by using pressure gauge (Omega) and digital manometer (Dwyer).

A typical experimental run was initiated with the pre-heating of gasifier, syngas purification system and all connecting lines to the designated operating temperatures. During heating, N₂ (300 mL/min) was purged into the gasifier to maintain an inert environment while a mixture of H₂ (50 mL/min) and N₂ (50 mL/min) was purged into the syngas purification system to maintain a reducing environment for the reduction of tar reforming catalyst and desulfurization sorbent.

Approximately 15 min before the start of experiment, purging of H₂ ceased while purging of N₂ continued to remove the H₂ and maintain an inert environment in the system. After pre-heating and stabilization of the temperature in gasifier, feeding of RDF pellets was started by using a screw-feeder which consisted of a fuel holder (mass capacity of 1.6 kg and volume capacity of 6 L) and a horizontal screw-conveyor (length of 380 mm and diameter of 50 mm). As the screw-conveyor turned, RDF pellets were crushed, compacted and pushed to the top of the gasifier. RDF then dropped from the top towards the bottom of the gasifier and onto a stainless-steel mesh which acted as a support for the formation of char bed. Simultaneously, air was fed by using a mass flow controller (FMA5500A, Omega) through a circular distributor near the central region of the gasifier, positioned at ~10–15 cm above the char bed and water was injected using a peristaltic pump (Masterflex L/S®, Cole Palmer) through a coiled stainless-steel pipeline. Water was heated along the pipeline and evaporated into steam when entering the gasifier. Two thermocouples (TC1 and TC2) were placed at the center of gasifier and char bed, respectively, to measure real-time temperature profiles inside the gasifier. The height of the gasifier was 585 mm and the char bed was positioned at 105 mm from the bottom of the gasifier. After the stabilization of syngas composition, raw syngas was directed into the purification system.

2.5. Sampling and analysis

During the experiments, sampling of syngas components was carried out at the outlets of the downdraft gasifier (GS), tar reformer (TR) and desulfurization reactor (DES). Syngas, tar, chlorides (e.g. NaCl and KCl), HCl, sulfur species, H₂O, particulates were collected, analyzed and quantified. All sampling pumps (GilAir Plus, Sensidyne) and mass flow controllers were calibrated by using a bubble flow meter and checked during the experiments. Results were reported as averages \pm standard deviations (SDs) of three runs. 2-sample *t*-test was carried out using Minitab® 17 to determine the statistical significance of the experimental results.

Sampling of tar was carried out using two different methods for comparison and complementary data collection. Method I is a modified method with a series of sampling traps using isopropanol (IPA) as

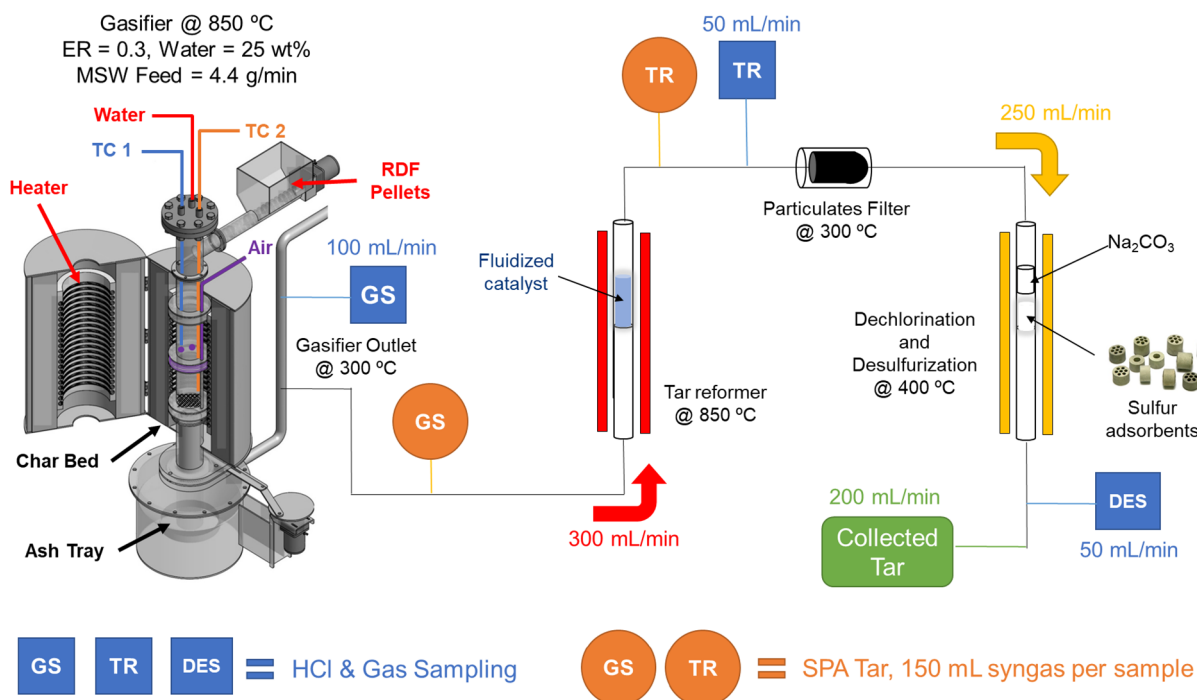


Fig. 1. Illustration of the hot syngas purification system integrated with downdraft gasification of municipal solid waste.

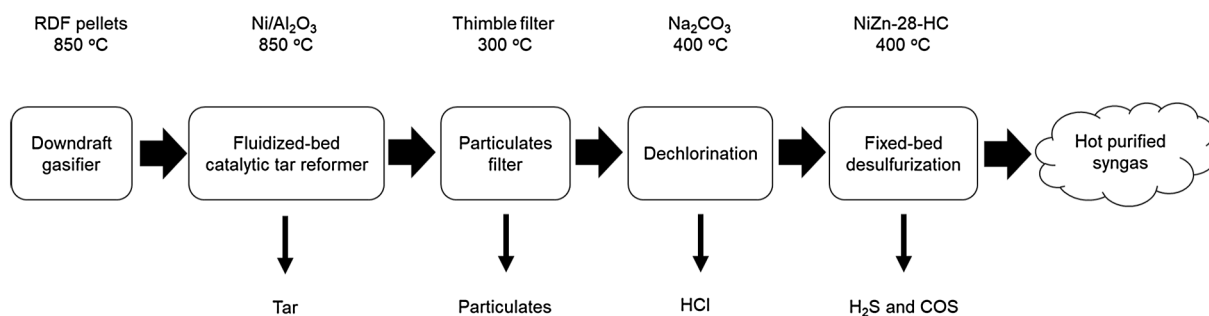


Fig. 2. Flow diagram of the hot syngas purification system integrated with downdraft gasification of municipal solid waste. Materials, operation temperatures and impurities removed are indicated.

solvent based on previous report [39]. The sampling train included a quartz thimble filter, connecting lines, five impinger bottles filled with 50 mL of IPA each and one empty impinger bottle. The second, fourth, fifth and the sixth impinger bottles were equipped with fine-meshed frits to produce smaller gas bubbles and to improve efficiency of tar capture by IPA. All the parts were rinsed with IPA after the sampling. Soxhlet extraction was used to dissolve tar compounds accumulated on the thimble filter with 250 mL IPA. All the collected IPA solutions were homogenized in a volumetric flask, topped up to 1 L, and denoted as “collected tar”. Method II utilized solid phase adsorption (SPA) by using tubes loaded with 500 mg of aminopropyl-bonded silica gel (Bond Elut NH₂, Agilent) [40]. Approximately 150 mL of syngas was directed through a SPA tube by using a sampling pump. Tar sampling was carried out at 30 min intervals simultaneously before and after the catalytic tar reformer (GS and TR sampling points, respectively). After sample collection, SPA tubes were sealed and stored in a dark cold room at 4 °C for 24 h before elution and analysis. A mixture of dichloromethane, acetonitrile and IPA with a volume ratio of 8:1:1 was used to extract polar and non-polar tar compounds simultaneously from the SPA tubes [41]. The tar analyzed by Method II is denoted as “SPA tar”.

Collected tar was sampled continuously throughout the experiment while SPA tar was sampled intermittently at selected time points. Therefore, collected tar represents the cumulative tar content while SPA tar represents instantaneous tar contents at different sampling times. Since the volume of IPA for Method I was 1 L, a large volume of syngas was needed to pass through the series of sampling traps to accumulate sufficient amount of tar for detection and quantification. In contrast, by Method II, small amount of syngas was required as only 2 mL of solvent was needed for tar extraction from SPA tubes. Method II is therefore simpler and faster as compared to Method I. In addition, SPA tar collection could detect the evolution of tar in the syngas during the experiments and occasional escape of tar compounds from the catalytic tar reformer.

Quantification of tar compounds in collected tar and SPA tar was carried out by using GC–MS (HP7890 GC with a 59751 MS, Agilent). The gas chromatograph was equipped with a HP-INNOWAX capillary column (i.d. of 0.250 mm and a film thickness of 0.25 μm). Chromatograms were recorded in total ion current (TIC) mode and peaks were identified by comparing their mass spectra to the NIST 11 mass spectra library. 33 tar compounds were quantitatively analyzed. The quantified tar compounds are showed in Table S2. Deuterated d8-toluene and d8-naphthalene were applied as internal standards for the analysis of all samples. The sum of concentrations of all tar compounds detected by GC–MS is denoted as total tar. Tar dew point, defined as the temperature at which the real total partial pressure of tar and the saturation pressure of tar are equal, was calculated based on the model developed by Energieonderzoek Centrum Nederland (ECN) and the concentrations of 34 individual tar components [42]. Tar removal (%) was calculated from the tar contents in raw and treated syngas (Tar_{raw} and $Tar_{treated}$) respectively:

$$Tar_{removal} (\%) = [(Tar_{raw} - Tar_{treated})/Tar_{raw}] \times 100\% \quad (1)$$

To analyze HCl and the main gases, syngas was pumped through two impinger bottles with deionized water to absorb HCl and then passed through a trap with silica gel to remove moisture and collect dry gas into a gas bag. Concentration of HCl in syngas was calculated based on the content of chloride anion (mg/L) in water traps analyzed by ion chromatograph (ICS-1100, Dionex). The content of cations (K⁺ and Na⁺) was measured using ICP-OES (Optima 8300, Perkin Elmer). The amount of Cl⁻ associated with K⁺ and Na⁺ was calculated and deducted from total Cl⁻ measured to quantify the concentration of HCl. The collected syngas was analyzed by a GC (7890B GC system, Agilent) coupled with two thermal conductivity and one flame ionization detectors. Details of quantified gas components are showed in Table S4.

Volume of the generated syngas is estimated based on the fraction of N₂ in air and syngas, respectively, and assuming that of N₂ is inert during the gasification and syngas purification. Output of syngas was then calculated as follows:

$$N_{2input} (Nm^3) = Air_{input} (Nm^3) \times \text{Fraction of } N_2 \text{ in air} \quad (2)$$

$$Syngas_{output} (Nm^3) = N_{2input} (Nm^3) \times \text{Fraction of } N_2 \text{ in syngas} \quad (3)$$

where $Syngas_{output}$ is the output of syngas on a dry basis, Air_{input} is the input of air and N_{2input} is the amount of N₂ in air.

Lower heating value (LHV) and cold gas efficiency (CGE) of syngas were calculated based on the heating values of the components in syngas (Table S5):

$$CGE = LHV_{output}/LHV_{input} \times 100\% \quad (4)$$

$$LHV_{output}(MJ) = LHV_{syngas}(MJ/Nm^3) \times Syngas_{output}(Nm^3) \quad (5)$$

$$LHV_{input}(MJ) = LHV_{RDF}(MJ/kg) \times Mass_{RDF}(kg) \quad (6)$$

where LHV_{output} is the total energy output in the syngas and LHV_{input} is the total energy input into the gasifier through RDF.

For the quantification of sulfur species (H₂S and COS), the collected syngas was analyzed by a GC (7890B, Agilent) equipped with a flame photometric detector. The content of particulates was calculated from the mass of quartz thimble filter (dried at 105 °C for 24 h) before and after each experiment. Solid residues remained in the gasifier after the experiments including char on the char bed, ashes in the ash tray and deposits on the inner wall of gasifier were collected, weighed and characterized.

2.6. Thermodynamic modeling

Thermodynamic modeling was carried out by using HCS Chemistry 9.0 (GEM, Outotec) which applied Gibbs energy minimization method to calculate the contents of CO, CO₂, CH₄, H₂, C₂–C₅ gases and H₂O at the equilibrium. The elemental composition of RDF pellets, amount of air input (ER = 0.3), water input (25 wt%), temperature (850 °C) and pressure (101.3 kPa) were used as the input parameters.

3. Results and discussion

3.1. RDF gasification and properties of raw syngas

Temperature profiles of the oxidation (near air distributor) and reduction (char bed on the stainless-steel mesh) regions as denoted by TC1 and TC2 are illustrated in Fig. S1. Based on the smaller standard deviations, relatively consistent temperatures were observed in the oxidation zone ($883 \pm 8^\circ\text{C}$) compared to the reduction zone ($873 \pm 22^\circ\text{C}$). The production and composition of raw and treated syngas were generally stable as illustrated in Fig. 3a for raw syngas and Fig. 3b for treated syngas. The syngas generated from the gasifier, consisted of $13 \pm 2\text{ vol}\%$ CO, $11 \pm 0.4\text{ vol}\%$ CO₂, $3.2 \pm 0.2\text{ vol}\%$ CH₄, $12 \pm 2\text{ vol}\%$ H₂, $2.9 \pm 0.3\text{ vol}\%$ C₂-C₅ gases and $58 \pm 4\text{ vol}\%$ N₂ (Fig. 4a), with a syngas yield (dry basis) of 2.7 ± 0.3 and $1.1 \pm 0.2\text{ Nm}^3/\text{kg}$ of RDF with and without N₂, respectively. LHV of the raw syngas was $6.7 \pm 1.6\text{ MJ}/\text{Nm}^3$ while the CGE of this allothermal gasifier was $79 \pm 20\%$. Moisture content (wet basis) in syngas generated from gasifier was $23 \pm 4\text{ vol}\%$ while the particulates content was $1.9 \pm 1.2\text{ g}/\text{Nm}^3$. Collected and SPA tar contents (Table 1) in raw syngas were $7.8 \pm 3.7\text{ g}/\text{Nm}^3$ and $7.3 \pm 1.6\text{ g}/\text{Nm}^3$, respectively, suggesting no statistically significant difference between the two analytical methods. 25 different tar compounds (Table S3) were similarly identified in the collected and SPA tar from raw syngas. Toluene, styrene and naphthalene were the main tar compounds which accounted for $74 \pm 3\text{ wt}\%$ of total tar content. The contents of styrene in collected and SPA tar were $1.4 \pm 0.8\text{ g}/\text{Nm}^3$ and $1.7 \pm 0.5\text{ g}/\text{Nm}^3$, respectively. This is different from the syngas generated during biomass gasification, in which styrene is a minor tar component [13]. Formation of styrene could be attributed to the presence of polystyrene in the MSW [43].

The content of solid residues, which were mixtures of char from the char bed, ashes from the ash tray and deposits on the inner wall of the gasifier, was $15 \pm 4\text{ wt}\%$ (based on the total amount of RDF input). Characterization results showed that the solid residues consisted of $26 \pm 4\text{ wt}\%$ of C, $0.7 \pm 0.1\text{ wt}\%$ of H, $0.5 \pm 0.1\text{ wt}\%$ of N, $0.4 \pm 0.1\text{ wt}\%$ of S, $5 \pm 3\text{ wt}\%$ of O (calculated by difference), $68 \pm 4\text{ wt}\%$ of ashes, and $4 \pm 0.5\text{ wt}\%$ Cl. Syngas, tar and solid residues contained $84 \pm 12\%$, $6 \pm 1\%$ and $4 \pm 2\%$ of total carbon, respectively, and carbon balance closure was $94 \pm 12\%$.

After the correction for chlorine content contributed by the alkali chlorides, the HCl content in syngas was $0.26 \pm 0.15\text{ g}/\text{Nm}^3$ as showed in Table 3. Concentrations of KCl and NaCl were $0.44 \pm 0.17\text{ g}/\text{Nm}^3$ and $0.56 \pm 0.23\text{ g}/\text{Nm}^3$ respectively. Mass ratio for K:Na was approximately 1:1. HCl, KCl, and NaCl in raw syngas accounted for $9 \pm 5\%$, $7 \pm 3\%$ and $11 \pm 5\%$ of total Cl, respectively, while the solid residues contained for $55 \pm 16\%$ of total Cl. Therefore, $82 \pm 18\%$ closure of Cl mass balance was achieved. The losses of Cl could be attributed to the condensation of alkali chlorides in the pipes and reactors.

Approximately 80 ppmv of sulfur species (H₂S and COS), as showed in Table 2, were detected in the syngas generated from the gasifier. Evolution profiles of H₂S and COS during a typical experiment carried out in the experimental set-up are presented in Fig. S2. Concentration of COS in raw syngas was higher compared to that of commonly reported for biomass and coal syngas, in which H₂S is the main sulfur compound [44], which can be attributed to the differences in the characteristics of feedstock and produced syngas [45]. Nevertheless, comparable poisoning effects on the Ni catalysts by H₂S and COS were previously reported [46]. Therefore, the Ni catalysts treating raw syngas from MSW gasification were required to be strongly resistant to both sulfur species and in this case, the total amount of sulfur species should be considered as a crucial parameter, equally important as the concentrations of individual sulfur compounds in the syngas.

3.2. Fluidized bed tar reforming

Since the temperature of syngas at the outlet of gasifiers is typically high, it is energetically favorable to carry out tar reforming without cooling down of syngas. In addition, it is important to carry out catalytic tar reforming at temperature higher than 800°C to suppress the poisoning effect of sulfur species on the Ni catalysts [47]. Although the removal of particulates prior to tar reformer would be beneficial [48], filter materials that can operate at such high temperatures are still under development [49]. Therefore, a fluidized-bed catalytic tar reformer was applied in the purification system to avoid plugging caused by particulates in raw syngas. Pressure of the purification system was constant throughout the experiment suggesting no significant bed agglomeration and plugging when raw syngas was directed into tar reformer without any pre-treatment.

Experiments with an empty reforming reactor (empty reformer) showed that the total tar content (Table 1), composition of main gases (Fig. 4), gas yield and LHV (Fig. 5) of syngas were statistically similar to those of raw syngas. However, the number of detected tar compounds was reduced to 15 (Table S3) based on the results from collected tar samples. Styrene and some other tar compounds were partially decomposed, while the concentration of naphthalene significantly increased, indicating that thermal treatment changed the composition of tar due to thermal cracking and conversion of tar compounds to naphthalene. This is probably because of the high thermal stability of naphthalene as compared to other tar compounds [50]. In the presence of catalysts in the tar reformer, most of the tar compounds were reformed and the total tar contents in collected tar decreased to $0.8 \pm 0.3\text{ g}/\text{Nm}^3$ with 5 mL of F-Cat, suggesting up to 90% of tar removal efficiency (Table 1). The only tar compounds that were detected in the treated syngas were toluene, styrene and naphthalene, with toluene and naphthalene accounting for more than 95 wt% of the collected tar. These results suggest that further research should be carried

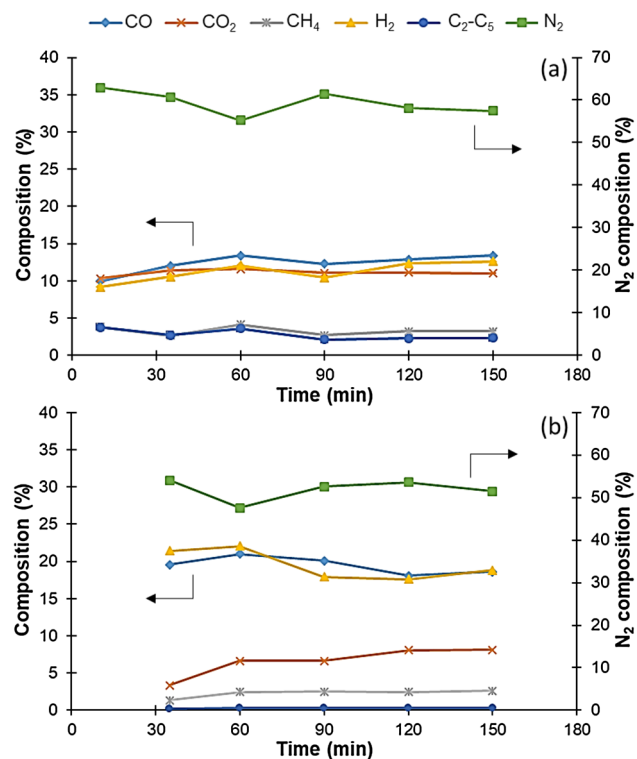


Fig. 3. Gas composition of (a) raw syngas collected from gasifier and (b) treated syngas after passing through the purification system during a typical experiment. The data are showed as averages of three runs.

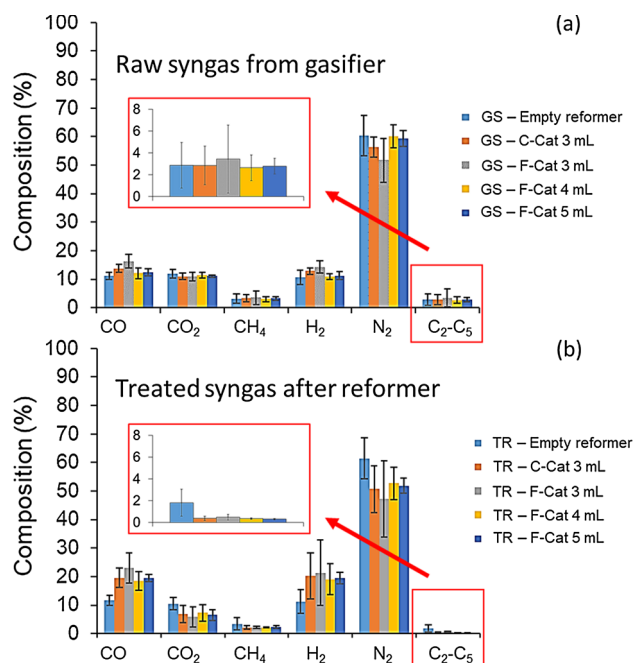


Fig. 4. Gas composition of (a) raw syngas generated from gasifier (GS) and (b) treated syngas after passing through tar reformer (TR) for five different sets of experiments, which included empty reformer (without catalyst) and catalytic tar reformer placed with C-Cat (3 mL) and F-Cat with different dosages (3 mL, 4 mL and 5 mL). The data are showed as averages \pm SDs of three runs.

out with the focus on the design of catalysts with high selectivity to the reforming of these two tar compounds. Fig. 6a presents the removal of collected tar and individual tar components using the F-Cat and C-Cat. The removal efficiency of the catalysts is plotted against NiO loading in the catalyst bed. Removal of total tar, toluene, naphthalene and styrene increased with the increased NiO loading from 0.38 to 0.51 g. The further increase in NiO loading did not decrease tar content significantly suggesting that the tar removal efficiency reached a plateau and could not be significantly improved with only the increment of NiO loading. Fig. 6b and 6c illustrate collected and SPA tar removal using 4 mL F-Cat (NiO loading of 0.51 g) for syngas reforming. F-Cat demonstrated operational stability in direct contact with the raw syngas for more than 20 h on stream (Fig. 6b). The fluctuations in removal

Table 1

GC-MS detectable tar in syngas from gasifier (GS), empty reformer (without catalysts) and after catalytic tar reforming (TR). Total tar, toluene, styrene and naphthalene contents (g/Nm^3) measured by using two different tar sampling methods, namely, collected and SPA tar. The corrected results for SPA tar based on the correlations between these two methods were presented.

Sampling method	Test	Tar content (g/Nm^3)							
		Total Tar		Toluene		Styrene		Naphthalene	
Collected tar	Gasifier	7.8	± 3.7	2.7	± 1.5	1.4	± 0.8	1.7	± 0.6
	Empty reformer	7.2	± 1.9	2.8	± 0.5	0.9	± 0.2	3.0	± 0.9
	C-Cat 3 mL	1.1	± 0.5	0.6	± 0.3	0.1	± 0.1	0.5	± 0.3
	F-Cat 3 mL	2.8	± 0.2	1.6	± 0.2	0.2	± 0.03	0.9	± 0.04
	F-Cat 4 mL	1.2	± 0.5	0.6	± 0.2	0.02	± 0.03	0.5	± 0.3
	F-Cat 5 mL	0.8	± 0.3	0.5	± 0.1	0.04	± 0.06	0.3	± 0.1
SPA tar	Gasifier	7.3	± 1.6	2.9	± 0.9	1.7	± 0.5	1.5	± 0.2
	C-Cat 3 mL	1.0	± 0.6	0.2	± 0.1	0.03	± 0.02	0.7	± 0.5
	F-Cat 3 mL	1.1	± 0.5	0.5	± 0.3	0.1	± 0.04	0.6	± 0.4
	F-Cat 4 mL	0.6	± 0.3	0.2	± 0.1	0.02	± 0.02	0.4	± 0.2
	F-Cat 5 mL	0.7	± 0.4	0.2	± 0.1	0.03	± 0.02	0.5	± 0.3
	Corrected SPA tar	C-Cat 3 mL	1.3	± 0.8	0.5	± 0.2	0.03	± 0.02	0.7
F-Cat 3 mL		2.1	± 0.9	1.5	± 0.6	0.1	± 0.04	0.6	± 0.4
F-Cat 4 mL		0.9	± 0.5	0.5	± 0.01	0.02	± 0.02	0.4	± 0.2
F-Cat 5 mL		0.9	± 0.5	0.4	± 0.03	0.03	± 0.02	0.5	± 0.3

Table 2

Sulfur species quantified in the syngas collected from gasifier (GS), after catalytic tar reformer with 4 mL of F-Cat (TR) and desulfurization reactor (DES).

Sulfur species	H_2S (ppmv)			COS (ppmv)		
	Mean	SD	RSD%	Mean	SD	RSD%
GS	14	2	12%	68	12	18%
TR	24	6	24%	72	34	48%
DES	0.1	0.2	173%	6	6	93%

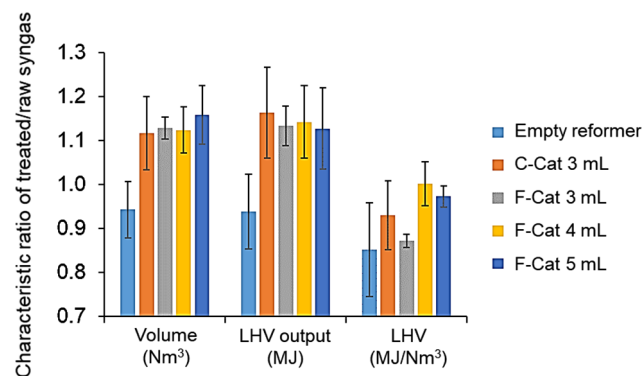


Fig. 5. Characteristic ratio of treated/raw syngas for volume of syngas (Nm^3), LHV output (MJ) and LHV (MJ/Nm^3). The data are showed as averages \pm SDs of three runs.

efficiencies during gasification runs could be observed using SPA tar samples (Fig. 6c). These fluctuations could be one of the reasons that reduced the overall tar removal efficiency.

It is important to assess the potential of using the treated syngas in real applications. The assessment was carried out based on the dew points and concentration limits of tar. Tar dew point is an important parameter to be considered for downstream applications of syngas [51]. Typically, the gas intake system of gas engine/turbine has to be maintained at approximately 28°C above the dew point of the syngas to avoid any condensation of tar [52]. The calculated tar dew point of the treated syngas was $22 \pm 6^\circ\text{C}$. Therefore, by maintaining the operating temperature of the gas intake system at around 50°C , the treated syngas is potentially usable in the gas engine/turbine. On the other hand, concentration limits set based on CEN/BT/TF 143 for different categories of tar compounds according to the number of carbon ring and

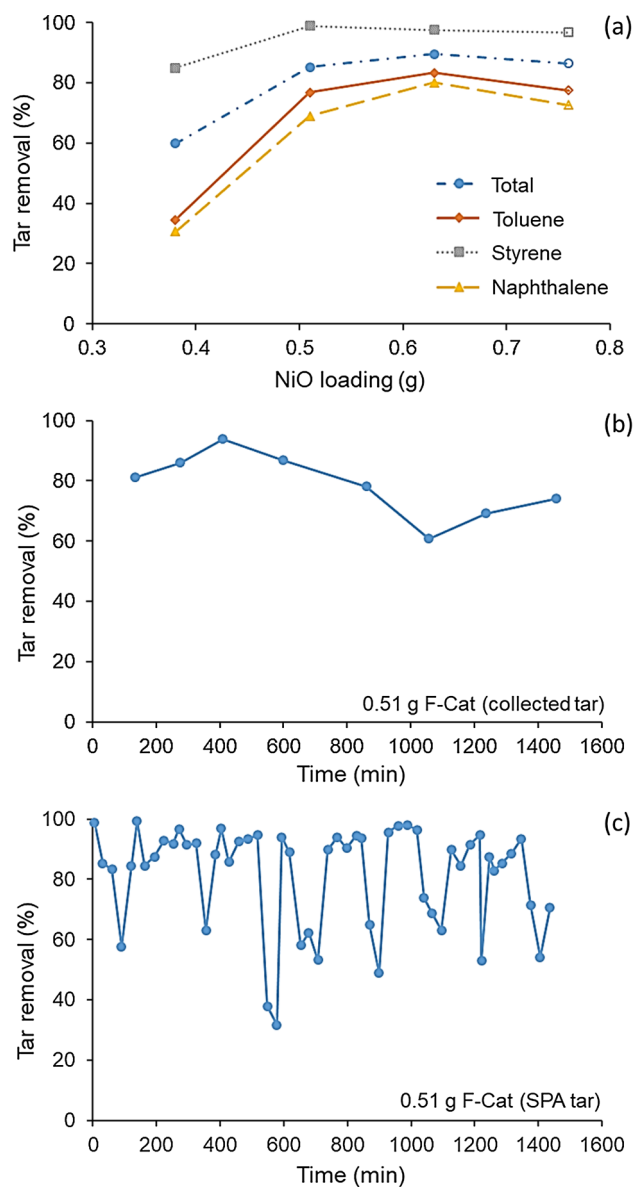


Fig. 6. (a) Removal of total tar and main tar components by catalytic tar reforming with 0.38, 0.51 and 0.63 g of F-Cat (closed symbols) and 0.76 g of C-Cat (open symbols). (b) Collected tar and (c) SPA tar removal over F-Cat.

molecular weight as showed in Table S6 suggested that the treated syngas could be applied in the gas engines/turbines [19]. The contents of one ring (toluene and styrene) and two rings (naphthalene) tar compounds in the treated syngas were 0.5 ± 0.2 and 0.3 ± 0.1 g/Nm³ respectively. These concentrations were lower than the equivalent limits of 9.5 and 1.3 g/Nm³ respectively. Alternatively, the treated syngas could be utilized in SOFC for electricity generation which demonstrated successful operation with the syngas consisted of 0.5–10 g/Nm³ of tar [53].

Nevertheless, it is still desirable to further reduce the tar content in the syngas to achieve high performance in the integrated gasification, purification and syngas utilization system. The improvement could be carried out by further testing of different dosages of catalysts, operating conditions of catalytic tar reformer, synthesis of novel catalysts and the addition of polishing unit employing adsorption/absorption techniques with the use char [54], activated carbon and waste oil [55].

In contrast to tar sampled at the outlet of gasifier (~300 °C, 101 kPa), statistically significant differences were observed for tar sampled at the outlet of the tar reformer after catalytic treatment

(~850 °C, 95 kPa) among the samples of collected and SPA tar. Differences between the data obtained from the two tar sampling methods for tar contents measured after catalytic tar reformer are illustrated in Fig. 7. Results showed that total tar contents estimated by using SPA were sometimes lower than the collected tar. Toluene contents were consistently lower in SPA than collected tar. Comparable styrene and naphthalene contents were observed for both methods. Correlation analysis revealed that the difference of total tar content estimated by these two methods could be primarily accounted by the difference between the toluene contents as illustrated in Fig. 8a, with a coefficient of determination (R^2) of 0.88. The loss of toluene could be attributed to the higher temperature and lower pressure at the sampling point after tar reformer which promote devolatilisation of the volatile organic and light tar compounds [56]. Nevertheless, the underestimation or loss of toluene content by SPA sampling method was closely correlated with the toluene content in syngas measured by using collected tar, as illustrated in Fig. 8b with a strong R^2 of 0.94. Therefore, tar sampling by SPA, though underestimated the contents of light tar compounds, could be corrected based on the supplementary results from collected tar and the corresponding correlation equations. The corrected results of SPA tar were comparable to collected tar as showed in Table 1. SPA can also be applied as a quick and simple tar measurement method for naphthalene or heavy tar compounds which can be used as representative indicators of tar contents in the syngas for an industrial environment. These results suggested that both methods are suitable for tar sampling. The selection of sampling method should then be subjected to the sampling need and the suitability of environment for setting up the sampling system.

Fig. 4b illustrates the compositions of main gases for catalytic tar reformer for different catalysts at different dosages. No statistically significant difference was observed in the composition of main gases, syngas yield and LHV when two catalysts at different loadings were used. In addition, the changes between compositions of raw and corresponding treated syngas were statistically comparable when two catalysts at different loadings were used. Therefore, the apparent differences among the experiments were due to the variations in the composition of raw syngas (Fig. 4a). To account for these variations and simplify the further discussion, an average of the composition of treated syngas from catalytic tar reformer with two catalysts at different dosages was calculated. In average, after catalytic tar reforming, syngas contained 20 ± 2 vol% CO, 7 ± 0.6 vol% CO₂, 2.2 ± 0.1 vol% CH₄, 20 ± 1 vol% H₂, 0.4 ± 0.1 vol% C₂-C₅ gases and 51 ± 2 vol% N₂. Moisture content in the treated syngas was reduced to 18 ± 5 vol%. Significant changes on the composition of main gases and moisture content suggest the presence of steam reforming reactions which convert tar compounds, CH₄ and C₂-C₅ gases into H₂ and CO. Concurrently, proportion of CO₂ was reduced (Fig. 4b) which could be attributed to the dry reforming reactions and the increased volume of the treated syngas (Fig. 5). Total volume of syngas (on a dry basis) increased by $14 \pm 5\%$ to 3.1 ± 0.4 Nm³/kg of RDF pellets. Average LHV of syngas decreased marginally from 6.7 ± 1.6 to 6.3 ± 1.4 MJ/Nm³ after catalytic tar reformer. The decreased in LHV can be attributed to the decreased contents of CH₄ and C₂-C₅ gases having relatively high LHVs as showed in Table S5. Total LHV output of the syngas increased by $14 \pm 8\%$ (Fig. 5). The estimated CGE of this system was $91 \pm 18\%$ after the allothermal catalytic tar reformer.

Based on thermodynamic modeling using Gibbs energy minimization method, the theoretical composition of syngas (on a dry basis) was 20.1 vol% CO, 7.4 vol% CO₂, 27.8 vol% H₂ and 44.7 vol% N₂. The contents of CH₄ and C₂-C₅ gases were negligible. The calculated LHV and yield of theoretical syngas were 5.5 MJ/Nm³ and 3.7 Nm³/kg respectively. Comparison of the properties of raw, treated and theoretical syngas at thermodynamic equilibrium showed that experimental and modeling results were different, suggesting the presence of kinetic constraints in the gasification and syngas purification system. Nevertheless, as compared to raw syngas, the composition of treated

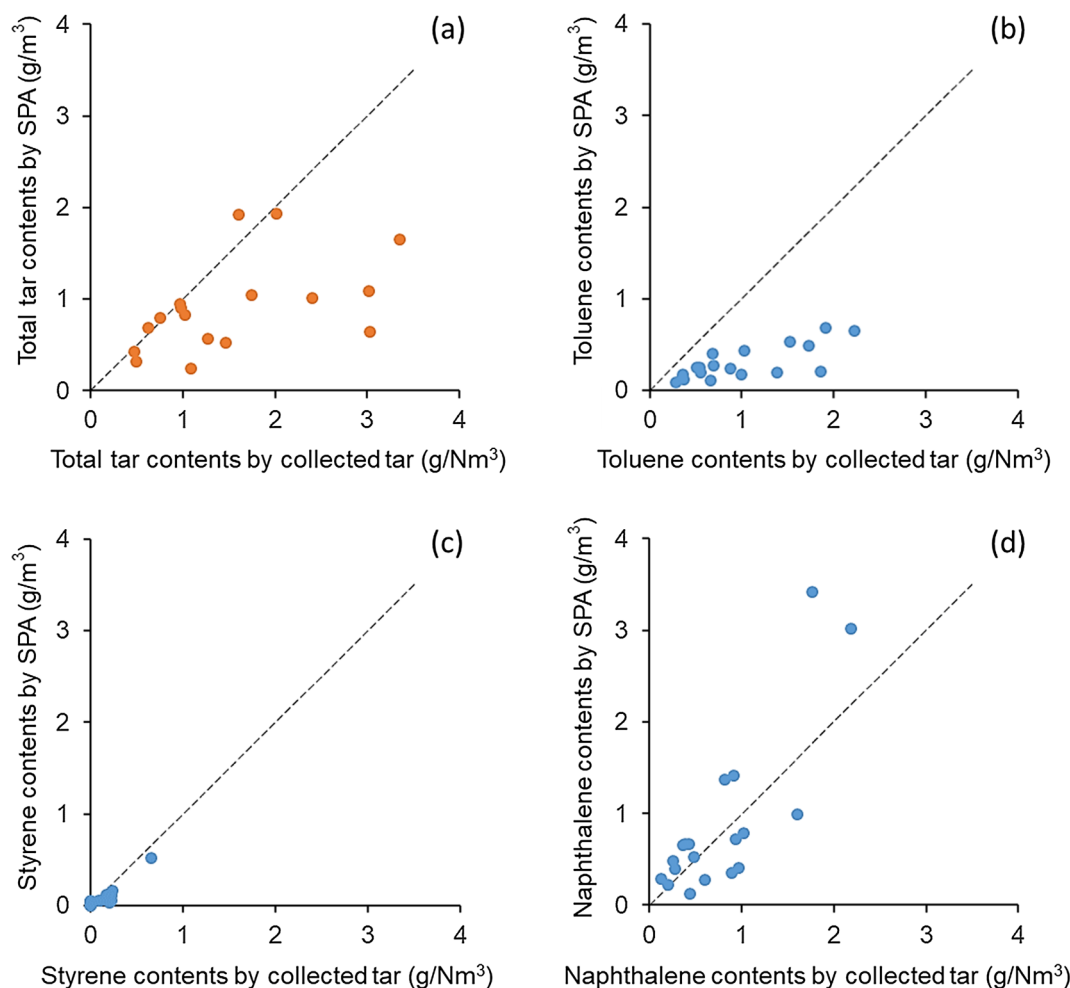


Fig. 7. Comparison of GC-MS detectable tar in syngas based on collected tar and SPA sampling methods. (a) Total tar, (b) toluene, (c) styrene and (d) naphthalene contents (g/Nm^3). Dotted lines indicated equivalent tar contents for both methods.

syngas was closer to the theoretical values (Table 4) suggesting that catalytic tar reforming helps in pushing the composition of syngas towards thermodynamic equilibrium. The main reason for the deviations between experimental results and calculations could be attributed to the kinetic constraints of H_2O related reactions because significantly higher amount of H_2O and lower amount of H_2 are present in the raw and treated syngas as compared to the theoretical values. Three potentially incomplete reactions were suggested which include steam reforming of tar, CH_4 and $\text{C}_2\text{-C}_5$ gases [57], water-gas shift reaction and gasification of particulates in syngas and solids residues remained in the gasifier. This is demonstrated by a three-step calculation of the yields (Nm^3/kg) for the main gases (Table 4) using treated syngas as the initial input. These calculation steps were carried out consecutively to reach the gas composition of theoretical syngas at equilibrium. Step 1, the yields were calculated by applying stoichiometric calculation and assuming complete steam reforming of the hydrocarbons (tar, CH_4 and $\text{C}_2\text{-C}_5$ gases) in the treated syngas. Step 2, using the calculated yields from Step 1 and thermodynamic modeling with Gibbs energy minimization method, conversion of H_2O and CO through water-gas shift reaction to produce H_2 and CO_2 at equilibrium was calculated. Step 3, using the calculated yields from Step 2 and stoichiometric calculation of steam and CO_2 gasification of carbon in the particulates in syngas and the solid residues remained in gasifier to produce H_2 and CO was carried out, by assuming that the equilibrium yields of H_2O and CO_2 were achieved. The final calculated values at Step 3 and modeling results showed good agreement. This observation supported the hypothesis on the kinetic constraints of H_2O related reactions and incomplete

gasification of solid residues. The kinetic constraints could be attributed to the low reactivity of char gasification with CO_2 and H_2O [58] and the poisoning of the catalysts by HCl [22] and sulfur species [59].

Concentrations of particulates in the syngas after passing through the catalytic tar reformer with 3 mL of C-Cat and 4 mL of F-Cat were 0.7 ± 0.3 and $0.8 \pm 0.8 \text{ g}/\text{Nm}^3$, respectively. Slight reduction of particulates in syngas after TR could be attributed to partial deposition of carbon and inorganic compounds over the catalysts and partial decomposition by gasification of residual solid carbon [15]. This observation is supported by the increase in sulfur species contents (Table 2), which probably originated from the decomposed particulates and the reduced content of chlorides (Table 3) in the treated syngas. Concentration of HCl after TR was $0.10 \pm 0.06 \text{ g}/\text{Nm}^3$. KCl and NaCl contents after TR were reduced to $0.08 \pm 0.08 \text{ g}/\text{Nm}^3$ and $0.10 \pm 0.10 \text{ g}/\text{Nm}^3$ respectively. The decrease in HCl , NaCl and KCl contents could be attributed to the deposition or adsorption of chlorides as reported previously for Ni-based sorbent [34] and alumina composites [60].

Approximately 90 ppmv of sulfur species (H_2S and COS), as showed in Table 2, were detected in the syngas after the catalytic tar reformer with 4 mL of F-Cat. Higher concentration of COS than H_2S was observed (Fig. S2), which is consistent with the distribution of sulfur species in the raw syngas. The slight increase of the total amount of sulfur species could be attributed to the conversion of sulfur-containing char and particulates into gases and partial hydrolysis or hydrogenation of COS to H_2S .

Since raw syngas was reformed directly in the catalytic tar reformer

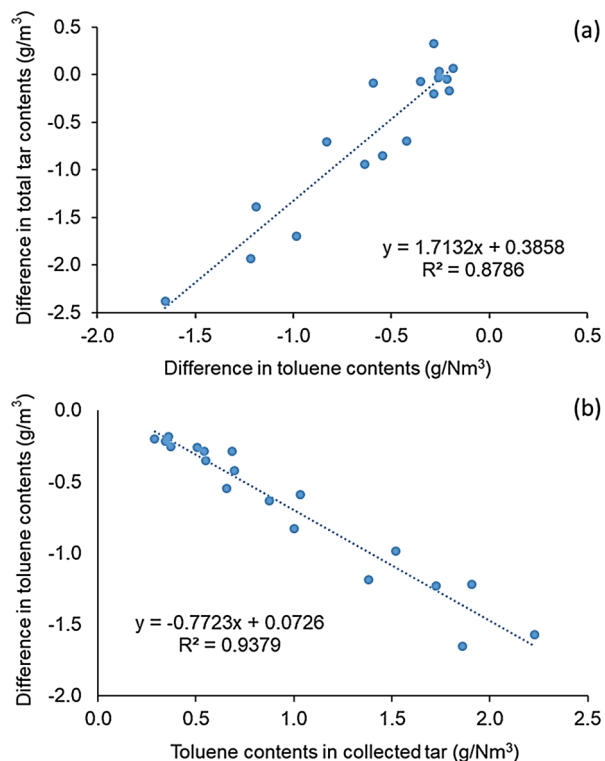


Fig. 8. (a) Correlation between difference ($Tar_{Difference} = Tar_{SPA} - Tar_{collected}$) in total tar and toluene contents measured by collected tar and SPA methods and (b) correlation between the difference of toluene contents ($Toluene_{Difference} = Toluene_{SPA} - Toluene_{collected}$) measured by the two methods and the toluene contents in collected tar.

Table 3

Chloride species quantified in the syngas collected from gasifier (GS) and after catalytic tar reformer with 4 mL of F-Cat (TR).

Chloride species	HCl			KCl			NaCl		
	Mean	SD	RSD%	Mean	SD	RSD%	Mean	SD	RSD%
GS	0.26	0.15	58%	0.44	0.17	39%	0.56	0.23	41%
TR	0.10	0.06	60%	0.08	0.08	100%	0.10	0.10	100%

without any pre-treatment, structural changes and properties of catalysts before and after the syngas purification were investigated. XRD patterns of the pristine and spent catalysts are showed in Fig. 9a. NiO diffraction peaks were identified on C-Cat. Absence of NiO peaks and presence of NiAl₂O₄ peaks could be observed at around 38°, 46° and 67°

Table 4

Average yield (Nm³/kg) of the main gaseous components in raw syngas from gasifier (GS), treated syngas (average of the treated syngas for different catalysts and different dosages) after catalytic tar reforming (TR) and the theoretical yield calculated based on a three steps calculation, (1) steam reforming of hydrocarbons, (2) water-gas shift reaction, (3) gasification of particulates and solid residues remained after gasification, and the thermodynamic equilibrium based on modeling.

Main gaseous component	Average yield (Nm ³ /kg)		Theoretical yield (Nm ³ /kg) based on a three steps calculation and thermodynamic modeling			
	GS Raw syngas	TR Treated syngas	Step 1 Steam reforming of tar, CH ₄ and C ₂ -C ₅ gases	Step 2 Water-gas shift reaction	Step 3 Gasification of particulates and solid residues	Modeling Thermodynamic equilibrium
CO	0.35	0.62	0.71	0.65	0.72	0.73
CO ₂	0.30	0.22	0.22	0.29	0.27	0.27
CH ₄	0.086	0.068	0	0	0	0
H ₂	0.32	0.62	0.88	0.95	0.98	1.0
N ₂	1.6	1.6	1.6	1.6	1.6	1.6
C ₂ -C ₅	0.078	0.012	0	0	0	0
H ₂ O	0.81	0.62	0.52	0.45	0.42	0.42

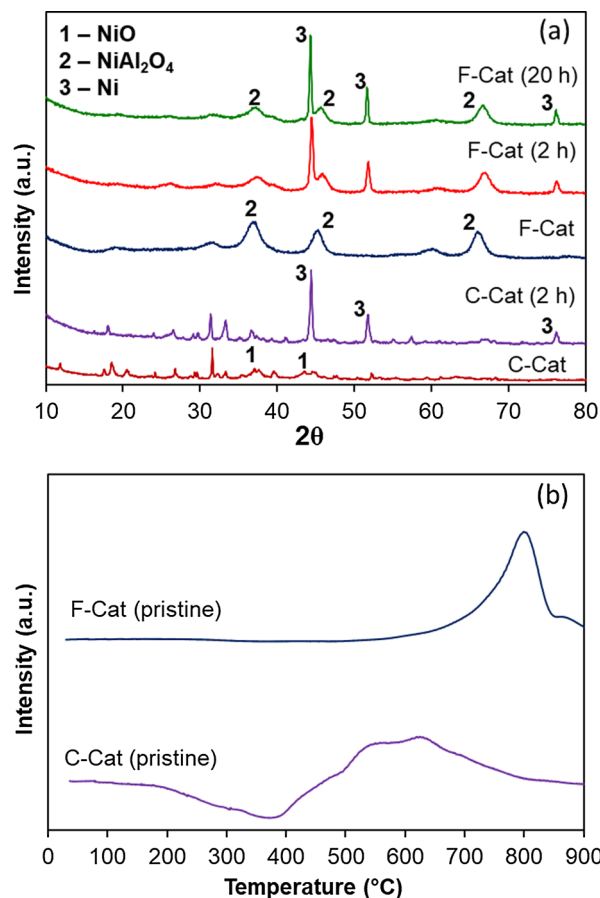


Fig. 9. (a) XRD patterns of pristine and spent catalysts, and (b) TPR profiles of pristine catalysts.

Table 5

CHN contents of catalysts before (pristine) and after being used in catalytic tar reformer (4 mL F-Cat and 3 mL C-Cat) for the treatment of raw syngas, for 2 and 20 h of operation.

Tar reforming catalysts		Mass %		
		C	H	N
F-Cat	Pristine	0	1.1	0.2
	2 h	10.4	0.9	0.2
	20 h	3.9	1	0.2
C-Cat	Pristine	2.7	1.7	0.2
	2 h	10.8	0.6	0.2

which could be explained by calcination at high temperature during synthesis (i.e. 850 °C) [61]. TPR profiles, as illustrated in Fig. 9b, also suggested that in the tested catalysts, nickel was present in different states. Reduction temperatures of oxidized nickel in C-Cat between 400 and 700 °C correspond to the reduction of NiO supported on Al₂O₃. The reduction peak at 780 °C in F-Cat is attributed to the reduction of NiAl₂O₄ spinel [62], which is consistent with the results of XRD analysis. In the spent C-Cat and F-Cat, metallic nickel formed via the reduction of NiO by syngas could be observed. The formation of other crystalline phases was not observed after 2 and 20 h of operation (catalysts C-Cat and F-Cat). The XRD patterns of F-Cat after 2 h and 20 h were similar indicating high structural stability of the catalyst in raw syngas during the operation. To investigate coke formation, the fresh and spent catalysts were characterized by elemental CHN analysis (Table 5). The two spent catalysts contained considerably high carbon contents of greater than 10.8% after 2 h of tar reforming, which is likely attributed to the presence of entrained char particles from gasifier. In the spent F-Cat catalyst, carbon content decreased with an increase in operation time from 2 to 20 h indicating that no continuous carbon deposition over time occurred and accumulated char particles could be removed from the catalyst bed via either attrition or steam and CO₂ gasification reactions [35]. The presence of low concentration of sulfur species (< 100 ppmv) in the raw syngas could also suppress the carbon formation reactions on the catalyst [63]. The morphology of different areas of spent F-Cat suggests that coking of catalyst mainly occurred on the Ni particles that were not strongly attached to the alumina support. Fig. 10a illustrates the formation of carbon nanofiber on such nanoparticle. On the other hand, no visible carbon deposition was detected on Ni nanoparticles that were embedded in the alumina support (Fig. 10b). As coking of catalysts is initiated with the deposition of carbon in the Ni lattice with the subsequent transfer to the Ni particle-support interface, strong interactions between Ni and the alumina support could prevent the uplifting of Ni particles and the subsequent growth of carbon fiber [64].

3.3. Desulfurization of syngas

Particulates filter and dechlorination sorbents were placed before NiZn-28-HC to remove particulates and HCl. Particulates can cause fouling and clogging in the fixed bed of desulfurization sorbent. HCl reacts with ZnO forming ZnCl₂ and decreasing sulfur capacity of the desulfurization sorbent [28]. Among the two tested dechlorination sorbents (i.e. CaO and Na₂CO₃), Na₂CO₃ had higher efficiency. This could be attributed to slower reaction rate between HCl and CaO, especially with the presence of higher CO₂ concentration in the syngas

that leads to carbonation reaction, as compared to more thermodynamically favorable and faster reaction of HCl with Na₂CO₃ [65].

Desulfurization reactor was maintained at 400 °C as the higher temperature could lead to thermodynamics limitations due to increased desorption rate of sulfur species. On the other hand, lower temperature could reduce the sorption rate of COS [34]. This is particularly important for the raw syngas generated from gasification of MSW due to the presence of COS at high concentrations. For syngas desulfurization, mean concentrations of H₂S and COS species, calculated based on triplicated experiments and total operation period of ~10 h, decreased to less than 10 ppmv in clean syngas after passing through the NiZn-28-HC sorbent (Table 2). This corresponds to more than 90% of total sulfur removal suggesting that the desulfurization of real syngas with the presence of small quantities of tar and significantly higher concentration of COS is practically feasible. The concentration of remaining sulfur compounds was below the acceptable levels for the operation of gas turbines (20 ppmv) [2], which makes NiZn-28-HC a promising sorbent for the purification of syngas at WtE plants integrated with CCGT. As the removal efficiency for H₂S was higher than 99% (Fig. S2), overall performance of desulfurization sorbent could be improved with the conversion of COS to form H₂S before desulfurization reactor. No statistically significant difference in the composition of main gases was observed before and after desulfurization reactor, indicating low catalytic activity of the sorbent at the utilized Ni-Zn loading and temperature.

XRD patterns of pristine and spent NiZn-28-HC after 2 h operation are illustrated in Fig. 11. Characteristic peaks for NiO ($2\theta = 38^\circ$ and 43°) and ZnO ($2\theta = 32^\circ$, 34° , 37°) were observed indicating the presence of both oxides in Ni-Zn nanocomposite. The overall peak intensity of spent NiZn-28-HC decreased and a hump between $2\theta = 25\text{--}40^\circ$ appeared after desulfurization, which could be attributed to the formation of amorphous ZnS [30]. High resolution XPS spectra of NiZn-28-HC at Zn 2p, Ni 2p, S 2p and Cl 2p regions are illustrated in Fig. 12. Characteristic binding energies of 1022 and 1045 eV for Zn 2p_{3/2} and Zn 2p_{1/2}, respectively, were observed indicating that no reduction of Zn occurred and oxidation state was Zn²⁺ for both pristine and spent sorbents [28]. Characteristic binding energies of 853, 856 and 862 eV for Ni 2p_{3/2} state could be attributed to Ni²⁺ (first two peaks) and a satellite peak, respectively [22]. Highly similar XPS spectra for Zn and Ni of both pristine and spent sorbents suggested high structural consistency before and after desulfurization. Characteristic binding energies for S 2p_{1/2} and S 2p_{3/2} at 163 and 162 eV, respectively, were observed indicating the sorption of sulfur species from the syngas while the presence of S⁶⁺ peak at 168 eV implied the formation of sulfate. The formation of sulfate could be due to the reaction between Ni-Zn oxides

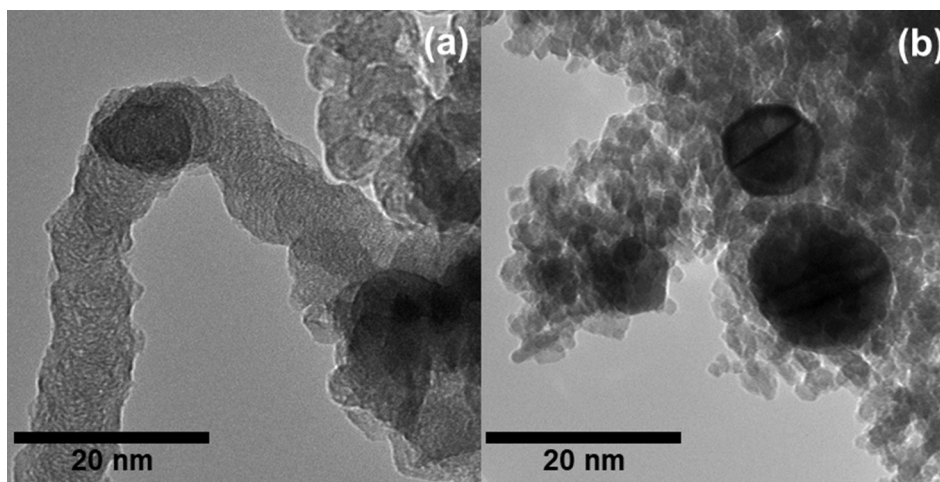


Fig. 10. TEM images of the spent F-Cat catalysts after 2 h operation: (a) deposition of filamentous carbon on a Ni nanoparticle loosely attached to the alumina support and (b) Ni nanoparticles embedded into alumina support with no visible carbon deposition.

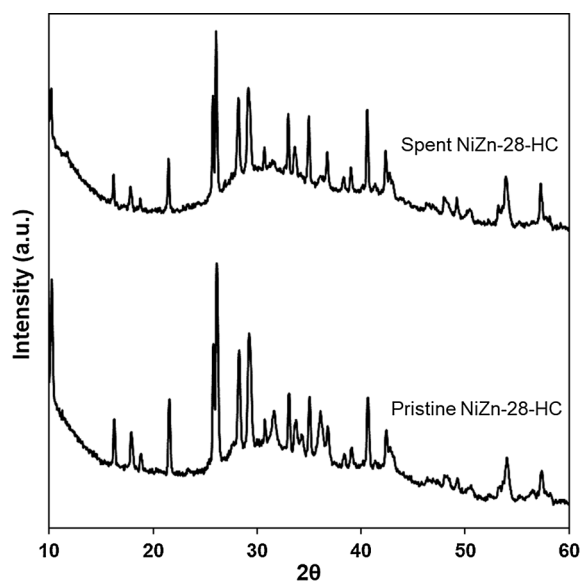


Fig. 11. XRD patterns of pristine and spent NiZn-28-HC.

and SO_2 or SO_3 species which were formed from the oxidation of H_2S with the Ni-Zn oxides [66]. This observation suggested that highly complex reactions could occur during the desulfurization of the real syngas with the formation of a variety of sulfur compounds such as sulfides and sulfates. Presence of Cl peaks in the region of 195–206 eV indicated that part of the Cl was adsorbed by the NiZn-28-HC which could be attributed to the incomplete HCl removal by Na_2CO_3 and/or the deposition of alkali chlorides present in syngas. This observation suggested that increased loading of Na_2CO_3 for HCl removal and/or utilization of sorbents for the removal of alkali chlorides could be beneficial for the operation of desulfurization sorbent. FESEM micrographs as shown in Fig. 13 illustrate the surface morphology of pristine and spent NiZn-28-HC. Based on the similar features, the structure of sorbent was not affected by the desulfurization of syngas. This could be attributed to the presence of Ni dopant which acted as a promoter to stabilize the lattice expansion and contraction effects [67]. Results of the characterization of the spent NiZn-28-HC showed high similarity with the results from a bench-scaled desulfurization set-up and suggested that the spent sorbent could be regenerated and reused as demonstrated previously [28].

In average, the amount of S captured by the NiZn-28-HC was estimated at 2.0 ± 0.8 mg/g of HC or equivalently, 113 ± 46 mg/g of Ni-Zn oxides. This is statistically comparable to the amount of S captured

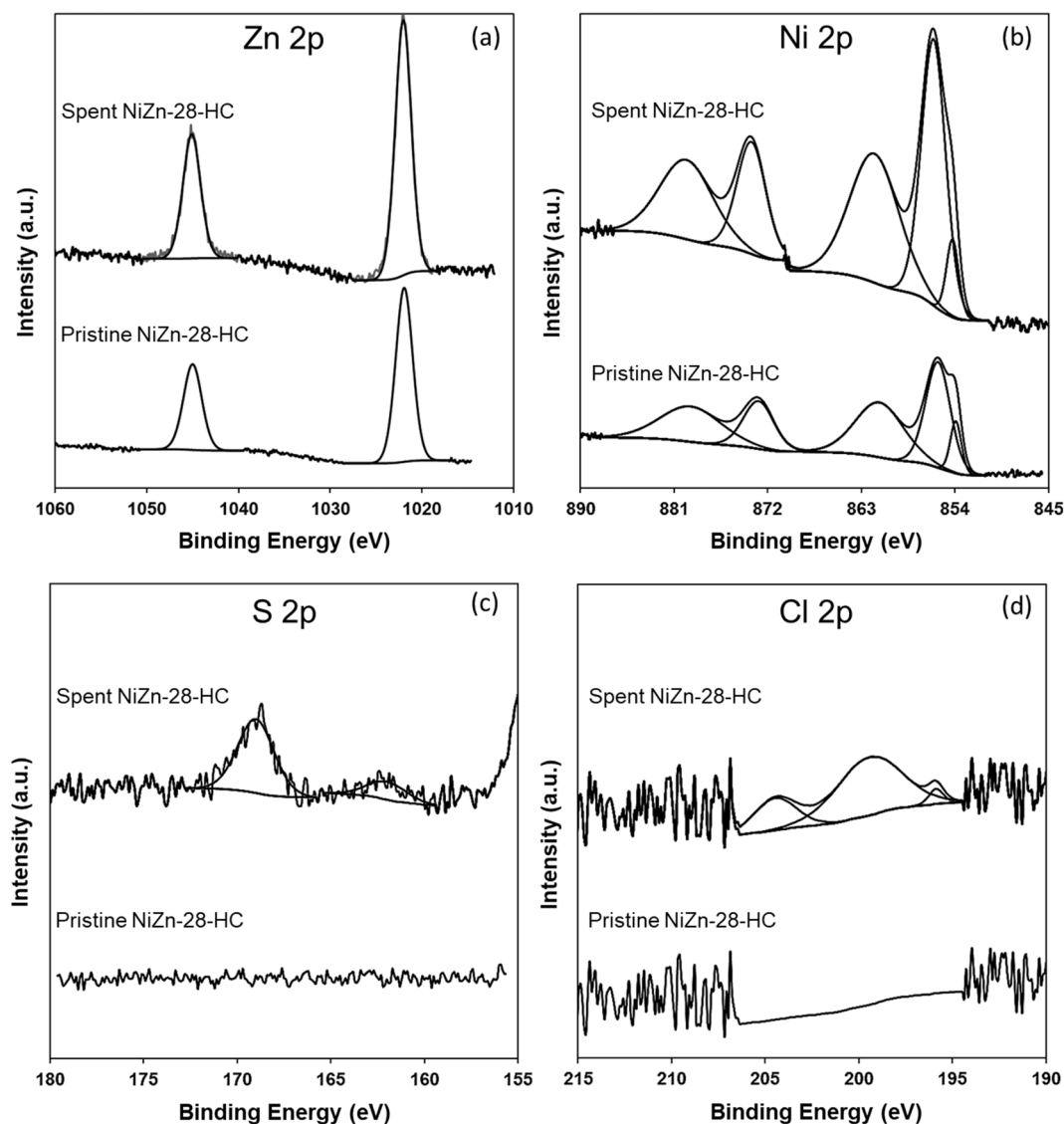


Fig. 12. High resolution XPS spectra at (a) Zn 2p, (b) Ni 2p, (c) S 2p and (d) Cl 2p for pristine and spent NiZn-28-HC.

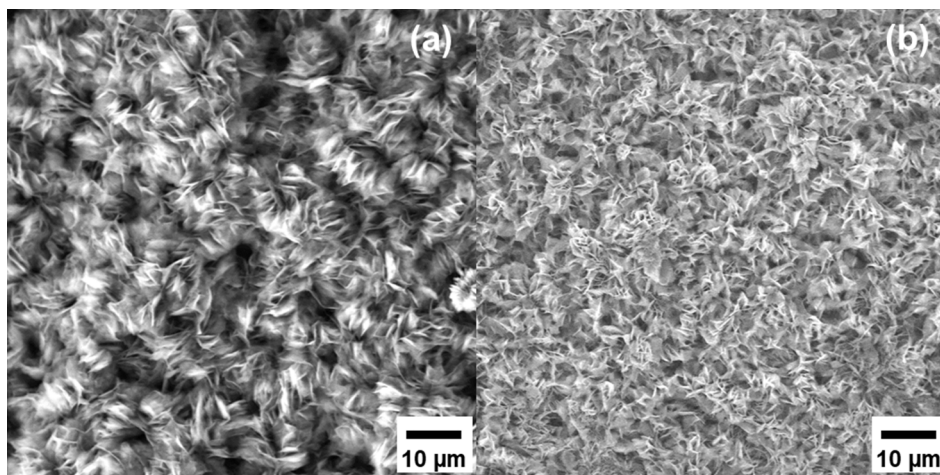


Fig. 13. FESEM micrographs of (a) pristine NiZn-28-HC after reduction and (b) spent NiZn-28-HC, top view.

by the same sorbents (159 ± 35 mg/g of Ni-Zn oxides) when tested using synthetic syngas (~ 100 ppmv S) as input in a bench-scale set-up [28]. This amount is calculated based on the total S removed when the outlet total S concentration for the bench-scale set-up reached 6 ppmv, similar to the concentration of S in the treated syngas as observed in this study. The slight reduction on the capturing of S could be attributed to the presence of higher concentration of COS (74 ppmv) and lower concentration of H_2S (24 ppmv) in real syngas as compared to the synthetic syngas which consists of predominantly H_2S (93 ppmv) and only traces of COS (7 ppmv). In addition, the incomplete HCl removal by Na_2CO_3 and/or the deposition of alkali chlorides present in real syngas could reduce the S removal capacity and efficiency.

4. Conclusions

A hot syngas purification system with downward cascading of syngas temperature was developed with satisfactory performance to treat raw syngas generated from downdraft gasification of real MSW and to produce clean syngas potentially applicable in more efficient downstream applications such as gas engines, CCGTs, SOFCs and hybrid energy recovery systems. Up to 90% removal efficiency of tar and sulfur compounds were achieved. Operational stability was demonstrated for the fluidized-bed catalytic tar reformer with nano-structured F-Cat treating dirty raw syngas directly from gasifier without any preliminary treatment. The strong resistance of catalyst to coking and poisoning could be attributed to the strong interactions between Ni particles and alumina support. Considering the tar dew point and specific concentration limits for different tar compounds, the treated syngas could be applied in the gas engines/turbines and SOFCs. Regenerable NiZn-28-HC desulfurization sorbent demonstrated excellent performance for syngas produced from MSW gasification, which consisted of significantly higher proportion of COS than H_2S and trace amounts of tar and HCl. Multiple impurities in raw and treated syngas were sampled and analyzed at different sampling points throughout this purification system and provided information on the evolution and distributions of these compounds. Comparison of the composition of raw and treated syngas with that at thermodynamic equilibrium provided insight into the differences between experimental and thermodynamic modeling results, particularly, on the kinetic constraints of steam reforming of hydrocarbons which include tar, CH_4 and C_2-C_5 gases, water-gas shift reaction and gasification of particulates in syngas and solid residues remained in the gasifier. These constraints could be caused by the poisoning of catalysts by the impurities (HCl and sulfur species) and the slow reaction kinetics between char, H_2O and CO_2 . Complementary and comparable results for tar contents were obtained by using two different tar sampling methods, namely collected tar and SPA tar,

indicating the applicability of both methods. Strong correlations were formed for these two methods to perform the correction of the loss of volatile tar compounds when the SPA sampling was carried out for a stream of syngas at higher temperature (~ 850 °C) and reduced pressure (~ 95 kPa), and in this case, toluene from SPA tar.

Acknowledgements

This research is supported by the National Research Foundation, Prime Minister's Office, Singapore and the National Environment Agency, Ministry of the Environment and Water Resources, Singapore, under the Waste-to-Energy Competitive Research Programme (WTE CRP 1501 105). The authors also acknowledge the management of Nanyang Environment and Water Research Institute and Economic Development Board, Singapore for the support.

Appendix A. Supplementary material

Supplementary data to this article can be found online at <https://doi.org/10.1016/j.apenergy.2019.01.031>.

References

- [1] Hoornweg D, Bhada-Tata P. What a waste: a global review of solid waste management. Urban development series; Knowledge papers No 15 World Bank, Washington, DC; 2012.
- [2] Arena U. Process and technological aspects of municipal solid waste gasification. A review. *Waste Manage* 2012;32:625–39.
- [3] Murer MJ, Spliethoff H, de Waal CM, Wilpshaar S, Berkhout B, van Berlo MA, et al. High efficient waste-to-energy in Amsterdam: getting ready for the next steps. *Waste Manage Res: J Int Solid Wastes Publ Cleansing Assoc ISWA* 2011;29:20–9.
- [4] Baskoro L, Muhammad A, Yoshikawa K, Takahashi F. Energy and resource recovery from Tetra Pak waste using hydrothermal treatment. *Appl Energy* 2017;207:107–13.
- [5] Shen Y, Yoshikawa K. Recent progresses in catalytic tar elimination during biomass gasification or pyrolysis—a review. *Renew Sustain Energy Rev* 2013;21:371–92.
- [6] Ebrahimi M, Moradpoor I. Combined solid oxide fuel cell, micro-gas turbine and organic Rankine cycle for power generation (SOFC–MGT–ORC). *Energy Convers Manage* 2016;116:120–33.
- [7] Pan Z, Liu Q, Zhang L, Zhang X, Chan SH. Effect of Sr surface segregation of $La_{0.6}Sr_{0.4}Co_{0.2}Fe_{0.8}O_{3-\delta}$ electrode on its electrochemical performance in SOC. *J Electrochem Soc* 2015;162:F1316–23.
- [8] Pålsson J, Selimovic A, Sjunnesson L. Combined solid oxide fuel cell and gas turbine systems for efficient power and heat generation. *J Power Sources* 2000;86:442–8.
- [9] Azizi MA, Brouwer J. Progress in solid oxide fuel cell-gas turbine hybrid power systems: system design and analysis, transient operation, controls and optimization. *Appl Energy* 2018;215:237–89.
- [10] R-z Zhang, Y-h Luo, R-h Yin. Experimental study on dioxin formation in an MSW gasification-combustion process: an attempt for the simultaneous control of dioxins and nitrogen oxides. *Waste Manage* 2018;82:292–301.
- [11] Zhou H, Meng A, Long Y, Li Q, Zhang Y. A review of dioxin-related substances during municipal solid waste incineration. *Waste Manage* 2015;36:106–18.
- [12] Torres W, Pansare SS, Goodwin JG. Hot gas removal of tars, ammonia, and

- hydrogen sulfide from biomass gasification gas. *Catal Rev* 2007;49:407–56.
- [13] Abdoulmoumine N, Adhikari S, Kulkarni A, Chattanathan S. A review on biomass gasification syngas cleanup. *Appl Energy* 2015;155:294–307.
- [14] Giuffrida A, Bonalumi D, Lozza G. Amine-based post-combustion CO₂ capture in air-blown IGCC systems with cold and hot gas clean-up. *Appl Energy* 2013;110:44–54.
- [15] Woolcock PJ, Brown RC. A review of cleaning technologies for biomass-derived syngas. *Biomass Bioenergy* 2013;52:54–84.
- [16] Higan C, van der Burgt M. *Gasification*. 2nd ed. Gulf Professional Publishing/Elsevier Science; 2008.
- [17] Moersch O, Spliethoff H, Hein KRG. Tar quantification with a new online analyzing method. *Biomass Bioenergy* 2000;18:79–86.
- [18] Valderrama Rios ML, González AM, Lora EES, Almazán del Olmo OA. Reduction of tar generated during biomass gasification: a review. *Biomass Bioenergy* 2018;108:345–70.
- [19] Fuel gas specifications – synthesis gas (syngas) IC-G-D-30-004e. Siemens; 2018.
- [20] Rakesh N, Dasappa S. A critical assessment of tar generated during biomass gasification – formation, evaluation, issues and mitigation strategies. *Renew Sustain Energy Rev* 2018;91:1045–64.
- [21] Yung MM, Jablonski WS, Magrini-Bair KA. Review of catalytic conditioning of biomass-derived syngas. *Energy Fuels* 2009;23:1874–87.
- [22] Veksha A, Giannis A, Oh W-D, Chang VWC, Lisak G, Lim T-T. Catalytic activities and resistance to HCl poisoning of Ni-based catalysts during steam reforming of naphthalene. *Appl Catal A* 2018;557:25–38.
- [23] Simell PA, Hepola JO, Krause AO. Effects of gasification gas components on tar and ammonia decomposition over hot gas cleanup catalysts. *Fuel* 1997;76:1117–27.
- [24] Shen Y, Zhao P, Shao Q, Takahashi F, Yoshikawa K. In situ catalytic conversion of tar using rice husk char/ash supported nickel-iron catalysts for biomass pyrolytic gasification combined with the mixing-simulation in fluidized-bed gasifier. *Appl Energy* 2015;160:808–19.
- [25] Zhang Z, Liu L, Shen B, Wu C. Preparation, modification and development of Ni-based catalysts for catalytic reforming of tar produced from biomass gasification. *Renew Sustain Energy Rev* 2018;94:1086–109.
- [26] Elbaba IF, Williams PT. High yield hydrogen from the pyrolysis-catalytic gasification of waste tyres with a nickel/dolomite catalyst. *Fuel* 2013;106:528–36.
- [27] Shen Y. Chars as carbonaceous adsorbents/catalysts for tar elimination during biomass pyrolysis or gasification. *Renew Sustain Energy Rev* 2015;43:281–95.
- [28] Oh W-D, Lei J, Veksha A, Giannis A, Chan W-P, Lisak G, et al. Ni-Zn-based nanocomposite loaded on cordierite mullite ceramic for syngas desulfurization: performance evaluation and regeneration studies. *Chem Eng J* 2018;351:230–9.
- [29] Ren Z, Guo Y, Liu C-H, Gao P-X. Hierarchically nanostructured materials for sustainable environmental applications. *Front Chem* 2013;1:18.
- [30] Oh W-D, Lei J, Veksha A, Giannis A, Lisak G, Chang VWC, et al. Influence of surface morphology on the performance of nanostructured ZnO-loaded ceramic honeycomb for syngas desulfurization. *Fuel* 2018;211:591–9.
- [31] Kong A, Wei Y, Li Y. Reactive adsorption desulfurization over a Ni/ZnO adsorbent prepared by homogeneous precipitation. *Front Chem Sci Eng* 2013;7:170–6.
- [32] Yongtao Y, Ning Ping, Guangfei Q, Junyan L, Qian Z. Remove sulfur dioxide from flue gases to obtain sulfuric acid through electro dialysis enrichment. *J Electrochem Soc* 2015;162. E141-E7.
- [33] Zhao H, Luo X, He J, Peng C, Wu T. Recovery of elemental sulphur via selective catalytic reduction of SO₂ over sulphided CoMo/γ-Al₂O₃ catalysts. *Fuel* 2015;147:67–75.
- [34] Spies KA, Rainbolt JE, Li XS, Braunberger B, Li L, King DL, et al. Warm cleanup of coal-derived syngas: multicontaminant removal process demonstration. *Energy Fuels* 2017;31:2448–56.
- [35] Trimm DL. Coke formation and minimisation during steam reforming reactions. *Catal Today* 1997;37:233–8.
- [36] Couté N, Richardson JT. Steam reforming of chlorocarbons: chlorinated aromatics. *Appl Catal B* 2000;26:217–26.
- [37] Albertazzi S, Basile F, Barbera D, Benito P, Brandin J, Einvall J, et al. Deactivation of a Ni-based reforming catalyst during the upgrading of the producer gas, from simulated to real conditions. *Top Catal* 2011;54:746.
- [38] Chan WP, Wang J-Y. Comprehensive characterisation of sewage sludge for thermochemical conversion processes – based on Singapore survey. *Waste Manage* 2016;54:131–42.
- [39] Neef JPA, Knoef HAM, Buffinga GJ, Zielke U, Sjöström K, Brage C, et al. Guideline for sampling and analysis of tars and particles in biomass producer gases. *Progress in thermochemical biomass conversion*. Blackwell Science Ltd; 2008. p. 162–75.
- [40] Brage C, Yu Q, Chen G, Sjöström K. Use of amino phase adsorbent for biomass tar sampling and separation. *Fuel* 1997;76:137–42.
- [41] Israelsson M, Seemann M, Thunman H. Assessment of the solid-phase adsorption method for sampling biomass-derived tar in industrial environments. *Energy Fuels* 2013;27:7569–78.
- [42] “Thersites”: website for tar dew point calculations. Energy research Centre of the Netherlands (ECN).
- [43] Sipra AT, Gao N, Sarwar H. Municipal solid waste (MSW) pyrolysis for bio-fuel production: a review of effects of MSW components and catalysts. *Fuel Process Technol* 2018;175:131–47.
- [44] Mondal P, Dang GS, Garg MO. Syngas production through gasification and cleanup for downstream applications — recent developments. *Fuel Process Technol* 2011;92:1395–410.
- [45] Wabash river coal gasification repowering project: a DOE assessment; 2002.
- [46] Jablonski WS, Villano SM, Dean AM. A comparison of H₂S, SO₂, and COS poisoning on Ni/YSZ and Ni/K₂O-CaAl₂O₄ during methane steam and dry reforming. *Appl Catal A* 2015;502:399–409.
- [47] Srinakruang J, Sato K, Vitidsant T, Fujimoto K. Highly efficient sulfur and coking resistance catalysts for tar gasification with steam. *Fuel* 2006;85:2419–26.
- [48] Aravind PV, de Jong W. Evaluation of high temperature gas cleaning options for biomass gasification product gas for Solid Oxide Fuel Cells. *Prog Energy Combust Sci* 2012;38:737–64.
- [49] Heidenreich S. Hot gas filtration – a review. *Fuel* 2013;104:83–94.
- [50] Tursun Y, Xu S, Wang G, Wang C, Xiao Y. Tar formation during co-gasification of biomass and coal under different gasification condition. *J Anal Appl Pyroly* 2015;111:191–9.
- [51] Provin D. TA 1000-0300 Fuel gas and combustion air requirements. GE Jenbacher GmbH & Co OG; 2015.
- [52] Meher-Homji CB, Zachary J, Bromley AF. Gas Turbine Fuels-System Design. Combustion: And Operability; 2010. p. 155–86.
- [53] Hofmann P, Panopoulos KD, Aravind PV, Siedlecki M, Schweiger A, Karl J, et al. Operation of solid oxide fuel cell on biomass product gas with tar levels > 10 g Nm⁻³. *Int J Hydrogen Energy* 2009;34:9203–12.
- [54] Nakamura S, Siritwat U, Yoshikawa K, Kitano S. Development of tar removal technologies for biomass gasification using the by-products. *Energy Procedia* 2015;75:208–13.
- [55] Phuphuakrak T, Namioka T, Yoshikawa K. Absorptive removal of biomass tar using water and oily materials. *Bioresour Technol* 2011;102:543–9.
- [56] Osipovs S. Comparison of efficiency of two methods for tar sampling in the syngas. *Fuel* 2013;103:387–92.
- [57] Násner AML, Lora EES, Palacio JCE, Rocha MH, Restrepo JC, Venturini OJ, et al. Refuse derived fuel (RDF) production and gasification in a pilot plant integrated with an Otto cycle ICE through Aspen plus™ modelling: thermodynamic and economic viability. *Waste Manage* 2017;69:187–201.
- [58] Li Z, Jiang L, Ouyang J, Cao L, Luo G, Yao H. A kinetic study on char oxidation in mixtures of O₂, CO₂ and H₂O. *Fuel Process Technol* 2018;179:250–7.
- [59] Mancino G, Cimino S, Lisi L. Sulphur poisoning of alumina supported Rh catalyst during dry reforming of methane. *Catal Today* 2016;277:126–32.
- [60] Fleming HL, Goodboy KP, Saforo EK. Adsorbent for HCl comprising alumina and acid-treated. Y zeolite 1985.
- [61] Li J, Yan R, Xiao B, Liang DT, Du L. Development of nano-NiO/Al₂O₃ catalyst to be used for tar removal in biomass gasification. *Environ Sci Technol* 2008;42:6224–9.
- [62] Sepehri S, Rezaei M, Garbarino G, Busca G. Facile synthesis of a mesoporous alumina and its application as a support of Ni-based autothermal reforming catalysts. *Int J Hydrogen Energy* 2016;41:3456–64.
- [63] Rostrup-Nielsen J, Christiansen LJ, Scientific W. Concepts in syngas manufacture, vol. 10 of catalytic science series. Imperial College Press; 2011.
- [64] Neagu D, Oh T-S, Miller DN, Ménard H, Bukhari SM, Gamble SR, et al. Nano-socketed nickel particles with enhanced coking resistance grown in situ by redox exsolution. *Nat Commun* 2015;6:8120.
- [65] Duo W, Kirkby NF, Seville JPK, Kiel JHA, Bos A, Den Uil H. Kinetics of HCl reactions with calcium and sodium sorbents for IGCC fuel gas cleaning. *Chem Eng Sci* 1996;51:2541–6.
- [66] de Falco G, Montagnaro F, Balsamo M, Erto A, Deorsola FA, Lisi L, et al. Synergic effect of Zn and Cu oxides dispersed on activated carbon during reactive adsorption of H₂S at room temperature. *Micropor Mesopor Mater* 2018;257:135–46.
- [67] Cheah S, Carpenter DL, Magrini-Bair KA. Review of mid- to high-temperature sulfur sorbents for desulfurization of biomass- and coal-derived syngas. *Energy Fuels* 2009;23:5291–307.